The Effect of Liquid Solidification on Turbulent Flow Heat Transfer of a Heat Generating Fluid in a Cold Tube

AUTHOR(S):

KIKUCHI, Yoshihiro; SHIGEMASA, Yasushi

CITATION:

KIKUCHI, Yoshihiro ...[et al]. The Effect of Liquid Solidification on Turbulent Flow Heat Transfer of a Heat Generating Fluid in a Cold Tube. Memoirs of the Faculty of Engineering, Kyoto University 1986, 48(2): 209-226

ISSUE DATE:

1986-05-17

URL:

http://hdl.handle.net/2433/281323

The Effect of Liquid Solidification on Turbulent Flow Heat Transfer of a Heat Generating Fluid in a Cold Tube

By

Yoshihiro KIKUCHI and Yasushi SHIGEMASA

(Received December 19, 1985)

Abstract

A theoretical study has been conducted to investigate the effect of liquid solidification (freezing) on the heat transfer characteristics for the turbulent flow of a heat generating fluid in a cooled circular tube. Steady-state conditions and a uniform wall temperature, which is lower than the liquid freezing temperature, are assumed. The radius of the liquid-solid interface and the local Nusselt number are determined as a function of position along the tube for several different values of the Reynolds number and the Prandtl number. The thickness of the frozen shell increases with distance down the tube. It approaches its fully developed value, depending upon a single dimensionless freezing parameter which measures the relative rate of wall cooling and internal heating. The local Nusselt number, however, first decreases rapidly and then approaches its fully developed value, which depends on the Reynolds number and the Prandtl number.

1. Introduction

The problems of the solidification (freezing) of liquids flowing inside cold channels have been encountered in numerous engineering applications. This type of solidification process is of recent interest because of nuclear reactor safety considerations. For example, a loss of coolant flow may result in the disruption of the reactor core that involves fuel melting. The molten fuel would flow upward and/or downward with solidification on cold core structures.

In a molten salt breeder reactor system, the fluorination of molten salt is required at several points in processes being considered for the isolation of protactinium and for the removal of rare earths. The fluorinators will be protected for corrosion by a layer of salt frozen on the metal surfaces that will potentially contact both the fluorine and molten salt[1]. The chemical reaction and the decay of fission products in the salt will constitute the heat source in the processing system.

In the current design of inertially confined fusion reactors[2], a thick liquid lithium falling curtain is used to protect the chamber wall from the micro-explosion

Department of Nuclear Engineering.

charged-particle energy deposition. If the falling curtain should be locally broken due to its flow instability, the charged particles will collide directly against the local portions of the wall, resulting in a local melting of the wall. We now propose an idea whereby the wall can be protected from charged-particle damage by a layer of frozen lithium formed on the wall, which is maintained at a desired temperature.

Despite its relevance to many important technological and physical problems, the solidification of a liquid as it flows through a cold channel has scarcely been studied, neither analytically nor experimentally. Most past studies[3-11] have been conducted in a fluid without internal energy sources. So far, there exist very few works, except the theoretical study of Kikuchi and Shigemasa[12], which treat the solidification of a heat generating fluid. This led the present authors to carry out a theoretical study for clarifying the effect of liguid solidification on heat transfer in a fluid with uniform energy sources flowing through a cooled tube under turbulent flow conditions. Simple analyses are presented for predicting the radius of the liquid-solid interface and the local Nusselt number. This paper is a sequal to the preceding report[12] which mainly covered the laminar flow case.

2. Analysis

2.1. Basic equations and assumptions

The liquid is assumed to have a uniform temperature T_0 and a fully developed turbulent velocity profile at the inlet where the cooling begins. Following this section, the tube wall is maintained at a constant temperature T_w, which is lower than the liquid freezing temperature T_f. The heat generating liquid is cooled as it flows down the tube, promoting solidification and thus causing the thickness of the frozen shell to increase with distance down the tube.

Fig. 1 illustrates the problem under consideration. The following assumptions are made in developing the formulation of the problem:

1. Steady-state conditions are maintained everywhere.

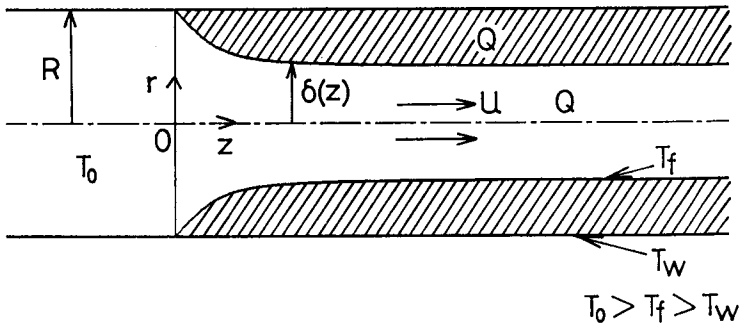

Fig. 1. Coordinate system.

2. The liquid flow is axisymmetric and turbulent, and has a fully developed velocity profile and a uniform temperature T_0 at the inlet ($z=0$).
3. The liquid is Newtonian and incompressible.
4. The physical properties of the liquid and solid phases are constant.
5. The solid phase is smooth, homogeneous and isotropic, and has a gradually increasing thickness beginning at the inlet.
6. The radial component of veloctiy due to the solid shell formation is neglected because the solid shell is thin. It is assumed that the fluid acceleration is not sufficiently strong to influence the structure of turbulent flow.
7. The temperature at the liquid-solid interface is constant and equal to the liquid freezing temperature T_f.
8. The wall temperature T_w is uniform, constant, and below the liquid freezing temperature.
9. Axial heat conduction, radiant heat transfer, and free convection are negligible.
10. The tube wall has negligible thermal resistance.
11. The volumetric heat generation is uniform and constant in the liquid and solid phases.

Under these assumptions the liquid-phase energy equation is written as

$$c\rho u\frac{\partial T}{\partial z}=\frac{1}{r}\frac{\partial}{\partial r}\left[k_l\left(1+\frac{\varepsilon_H}{a}\right)r\frac{\partial T}{\partial r}\right]+Q,\quad 0\leq r\leq\delta,\quad z\leq 0 \tag{1}$$

which is subject to the boundary conditions

$$T(\delta,\ z)=T_f \tag{2}$$

$$\frac{\partial T(0,\ z)}{\partial r}=0 \tag{3}$$

$$T(r,\ 0)=T_0 \tag{4}$$

The solid-phase energy equation, neglecting axial conduction, is given by

$$\frac{1}{r}\frac{\partial}{\partial r}\left(k_s r\frac{\partial T}{\partial r}\right)+Q=0,\quad \delta\leq r\leq R,\quad z\leq 0 \tag{5}$$

with boundary conditions

$$T(\delta,\ z)=T_f \tag{6}$$

$$T(R,\ z)=T_w \tag{7}$$

An additional relation necessary to determine $\delta(z)$ is an energy balance at the liquid-solid interface, i.e.

$$k_l\frac{\partial T_l(\delta,\ z)}{\partial r}=k_s\frac{\partial T_s(\delta,\ z)}{\partial r} \tag{8}$$

In order to simplify the description of the equations, the thermal conductivity of each phase is assumed to be the same. The following dimensionless quantities are introduced:

$$r^*=\frac{r}{R},\quad \delta^*=\frac{\delta}{R},\quad \eta=\frac{r}{\delta},\quad z^*=\frac{2z}{RePrR},\quad \Gamma=1+\frac{\varepsilon_H}{a},\quad \theta=\frac{T-T_f}{T_0-T_f},$$
$$\theta_w=\frac{T_f-T_w}{T_0-T_f},\quad Q^*=\frac{QR^2}{4k(T_0-T_f)},\quad u^*=\frac{u}{u_{m0}},$$
$$Re=\frac{2u_{m0}R}{\nu},\quad Pr=\frac{\nu}{a},\quad q^*=\frac{qR}{k(T_0-T_f)} \tag{9}$$

By utilizing these quantities, Eqs. (1) through (4) are transformed into the dimensionless forms

$$u^*\delta^{*2}\frac{\partial\theta}{\partial z^*}=\frac{1}{\eta}\frac{\partial}{\partial\eta}\left(\Gamma\eta\frac{\partial\theta}{\partial\eta}\right)+4Q^*\delta^{*2},\quad 0\leq\eta\leq1,\quad z^*\geq0 \tag{10}$$

$$\theta(1,\ z^*)=0 \tag{11}$$

$$\frac{\partial\theta(0,\ z^*)}{\partial\eta}=0 \tag{12}$$

$$\theta(\eta,\ 0)=1 \tag{13}$$

According to Assumption 6, the dimensionless velocity and total thermal diffusivity distributions are expressed by the following equations:

$$u^*(\eta,\ z^*)=u_0^*(\eta)/\delta^{*2} \tag{14}$$

$$\Gamma(\eta,\ z^*)=\Gamma_0(\eta) \tag{15}$$

where the subscript 0 refers to the value at the inlet. The expressions for u_0^* and Γ_0 are given in the Appendix.

Substituting Eqs. (14) and (15) into Eq. (10), we obtain

$$u_0^*\frac{\partial\theta}{\partial z^*}=\frac{1}{\eta}\frac{\partial}{\partial\eta}\left(\Gamma_0\eta\frac{\partial\theta}{\partial\eta}\right)+4Q^*\delta^{*2},\quad 0\leq\eta\leq1,\quad z^*\geq0 \tag{16}$$

The dimensionless forms of Eqs. (5) through (8) are expressed by the following equations

$$\frac{1}{\partial}\frac{\eta}{\partial\eta}\left(\eta\frac{\partial\theta}{\partial\eta}\right)+4Q^*\delta^{*2}=0,\quad 1\leq\eta\leq\frac{1}{\delta^*},\quad z^*\geq0 \tag{17}$$

$$\theta(1,\ z^*)=0 \tag{18}$$

$$\theta\left(\frac{1}{\delta^*},\ z^*\right)=-\theta_w \tag{19}$$

$$\frac{\partial\theta_l(1,\ z^*)}{\partial\eta}=\frac{\partial\theta_s(1,\ z^*)}{\partial\eta} \tag{20}$$

In the following analysis, the flow channel is separated into two regions: (1) a fully developed region and (2) a thermal entrance region. Calculation is then carried out for each region.

2.2. Fully developed region

In this region the solid layer thickness does not change and the liquid is isothermal along the axial direction. The left side of Eq. (16) is equal to 0. By solving this equation under the boundary conditions of Eqs. (11) and (12), we obtain the dimensionless liquid-phase temperature distribution

$$\theta=2Q^*\delta^{*2}\int_\eta^1\frac{\eta d\eta}{\Gamma_0} \tag{21}$$

The dimensionless solid-phase temperature distribution can be calculated from Eqs. (17) through (19) and is expressed by

$$\theta+\theta_w=Q^*(1-\delta^{*2}\eta^2)+[\theta_w-Q^*(1-\delta^{*2})]\left(1+\frac{\ln\eta}{\ln\delta^*}\right) \tag{22}$$

Substituting Eqs. (21) and (22) into Eq. (20) and considering that Γ_0 is equal to 1 at the liquid-solild interface, we obtain the dimensionless radius δ^* of the liquid-solid interface

$$\delta^*=\sqrt{1-\theta_w/Q^*}\equiv\sqrt{1-\phi} \tag{23}$$

where ϕ is the dimensionless freezing parameter, which measures the relative rate of wall cooling and internal heating.

With the relation of Eq. (23), the dimensionless solid-phase temperature distribution which is given by Eq. (22) becomes a simple form as

$$\theta+\theta_w=Q^*(1-r^{*2}) \tag{24}$$

The correlations of Eqs. (23) and (24) for the solid phase in turbulent flow are same as those as those in laminar flow, which are given in Ref. 12.

The dimensionless heat flux q^* at the liquid-solid interface can be determined from Eq. (21) and is given by

$$q^*=-\frac{1}{\delta^*}\frac{\partial\theta(1,\ z^*)}{\partial\eta}=2Q^*\delta^* \tag{25}$$

where Γ_0 is again taken as 1 at $\eta=1$.

Integration of Eq. (21) yields the dimensionless mixed mean temperature θ_m of the liquid phase as the following expression:

$$\theta_m=\frac{T_m-T_f}{T_0-T_f}=\frac{\int_0^1 2\pi\eta u^*\theta d\eta}{\int_0^1 2\pi\eta u^* d\eta}=4Q^*\delta^{*2}\int_0^1\eta u_0^*\left(\int_\eta^1\frac{\eta d\eta}{\Gamma_0}\right)d\eta \tag{26}$$

The fully developed Nusselt number Nu^{fd}, therefore, can be determined from Eqs. (25) and (26), and becomes as follows:

$$Nu^{fd}=\frac{2q\delta}{k(T_m-T_f)}=\frac{2q^*\delta^*}{\theta_m}=\frac{1}{\int_0^1\eta u_0^*\left(\int_\eta^1\frac{\eta d\eta}{\Gamma_0}\right)d\eta} \tag{27}$$

where the diameter 2δ of the flow area is taken as the representative length of the Nusselt number. The values of Nu^{fd} are functions of Re and Pr.

2.3. Thermal entrance region

In this region the liquid temperature is separated into two components

$$T=T^{fd}+T^e \tag{28}$$

By utilizing the following dimensionless quantities

$$\theta^{fd}=\frac{T^{fd}}{T_0-T_f},\quad \theta^e=\frac{T^e-T_f}{T_0-T_f} \tag{29}$$

Eq. (28) can also be transformed into the dimensionless form

$$\theta=\theta^{fd}+\theta^e \tag{30}$$

Each component satisfies the following energy equation and boundary conditions

$$\frac{1}{\eta}\frac{\partial}{\partial\eta}\left(\Gamma_0\eta\frac{\partial\theta^{fd}}{\partial\eta}\right)+4Q^*\delta^{*2}=0,\quad 0\leq\eta\leq1,\quad z^*\geq0 \tag{31}$$

$$\theta^{fd}(1,\ z^*)=0 \tag{32}$$

$$\frac{\partial\theta^{fd}(0,\ z^*)}{\partial\eta}=0 \tag{33}$$

and

$$u_0^*\frac{\partial\theta^e}{\partial z^*}=\frac{1}{\eta}\frac{\partial}{\partial\eta}\left(\Gamma_0\eta\frac{\partial\theta^e}{\partial\eta}\right),\quad 0\leq\eta\leq1,\quad z^*\geq0 \tag{34}$$

$$\theta^e(1,\ z^*)=0 \tag{35}$$

$$\frac{\partial\theta^e(0,\ z^*)}{\partial\eta}=0 \tag{36}$$

$$\theta^e(\eta,\ 0)=1 \tag{37}$$

By integrating Eq. (31) under the boundary conditions of Eqs. (32) and (33), we obtain

$$\theta^{fd}=2Q^*\delta^{*2}\int_\eta^1\frac{\eta d\eta}{\Gamma_0} \tag{38}$$

Eq. (34) can be solved under the boundary conditions of Eqs. (35) and (36) by a variable separation method and the solution is expressed by

$$\theta^e=\sum_{n=0}^{\infty}C_n\psi_n(\eta)\exp\left(-\frac{\lambda_n^2z^*}{2}\right) \tag{39}$$

where ψ_n and λ_n are the eigen-functions and eigen-values, respectively, of the following Sturm-Liouville problem

$$\frac{1}{\eta}\frac{d}{d\eta}\left(\Gamma_0\eta\frac{d\psi_n}{d\eta}\right)+\frac{u_0^*}{2}\lambda_n^2\psi_n=0 \tag{40}$$

$$\psi_n(0)=1 \tag{41}$$

$$\frac{d\psi_n(0)}{d\eta}=0 \tag{42}$$

$$\psi_n(1)=0 \tag{43}$$

To evaluate the coefficients C_n we apply the boundary condition of Eq. (37) which specifies the value at the inlet. Using the orthogonal property of the Sturm-Liouville system, we have

$$C_n=-\frac{\psi'_n(1)+4Q^*\int_0^1\eta\psi_n d\eta}{\int_0^1\Gamma_0\eta\psi_n'^2d\eta} \tag{44}$$

The complete soultion for the dimensionless liquid-phase temperature distribution is finally expressed by

$$\theta=2Q^*\delta^{*2}\int_\eta^1\frac{\eta d\eta}{\Gamma_0}+\sum_{n=0}^{\infty}C_n\psi_n(\eta)\exp\left(-\frac{\lambda_n^2z^*}{2}\right) \tag{45}$$

The dimensionless solid-phase temperature distribution is expressed by Eq. (22), which is the same in the fully developed region.

Substituting Eqs. (22) and (45) into Eq. (20), we obtain

$$\sum_{n=0}^{\infty} C_n \psi_n'(1) \exp\left(-\frac{\lambda_n^2 z^*}{2}\right) = \frac{\theta_w - Q^*(1-\delta^{*2})}{\ln \delta^*} \tag{46}$$

With this relationship of Eq. (46), the dimensionless radius δ^* of the liquid-solid interface can be calculated numerically.

The dimensionless heat flux q^* at the liquid-solid interface can be calculated from Eq. (45) and is given as

$$q^* = -\frac{1}{\delta^*}\frac{\partial \theta(1,\ z^*)}{\partial \eta} = 2Q^*\delta^* - \frac{1}{\delta^*}\sum_{n=0}^{\infty} C_n \psi_n'(1) \exp\left(-\frac{\lambda_n^2 z^*}{2}\right) \tag{47}$$

Integration of Eq. (45) yields the dimensionless mixed mean temperature θ_m of the liquid. From the properties of the Sturm–Liouville system we can then write for θ_m

$$\theta_m = \frac{\int_0^1 2\pi \eta u^* \theta d\eta}{\int_0^1 2\pi \eta u^* d\eta}$$

$$= 4Q^*\delta_*^2 \int_0^1 \eta u_0^* \left(\int_0^1 \frac{\eta d\eta}{\Gamma_0}\right) d\eta - 4\sum_{n=0}^{8} \frac{C_n}{\lambda_n^2} \psi_n'(1) \exp\left(-\frac{\lambda_n^2 z^*}{2}\right) \tag{48}$$

The local Nusselt number may be determined from the definition and written by

$$Nu = \frac{2q^*\delta^*}{\theta_m} = \frac{Q^*\delta^{*2} - \frac{1}{2}\sum_{n=1}^{\infty} C_n \psi_n'(1) \exp\left(-\frac{\lambda_n^2 z^*}{2}\right)}{Q^*\delta^{*2}\int_0^1 \eta u_0^* \left(\int_\eta^1 \frac{\eta d\eta}{\Gamma_0}\right) d\eta - \sum_{n=0}^{\infty} \frac{C_n}{\lambda_n^2} \psi_n'(1) \exp\left(-\frac{\lambda_n^2 z^*}{2}\right)} \tag{49}$$

The rate Q_T of heat transfer from the tube wall for the axial length z can be determined from the relation

$$Q_T = \int_0^z 2\pi R\left[-k\frac{\partial T(R,\ z)}{\partial r}\right] dz \tag{50}$$

By utilizing Eq. (22) and (46) and introducing the following dimensionless quantity

$$Q_T^* = \frac{Q_T}{\pi R^2 c\rho u_{m0}(T_0 - T_f)} \tag{51}$$

Eq. (50) can be transformed into the dimensionless form given by

$$Q_T^* = 4Q^*z^* + 4\sum_{n=0}^{\infty} \frac{C_n}{\lambda_n^2} \psi_n'(1) \left[\exp\left(-\frac{\lambda_n^2 z^*}{2}\right) - 1\right] \tag{52}$$

3. Results and discussion

3.1. Fully developed region

In order to establish a base case of fully developed heat transfer, calculations were first carried out for the non-generating fluid ($Q^*=0$) under the non-freezing condition ($\theta_w=0$). Some calculated results of the fully developed Nusselt number Nu^{fd} are listed in Table 1 for $Pr=1$ and for three Reynolds numbers. The calculated values of Nu^{fd} are slightly higher than the prediction from the conventional

Table 1. Fully developed Nusselt number for non-generating fluid of $Pr=1$ under non-freezing condition.

Investigators	$Re=5000$	$Re=10000$	$Re=50000$
Present authors	27	46	151
Dittus and Boelter	21	37	132

correlation of Dittus and Boelter[13]

$$Nu^{fd}=0.023\,Re^{0.8}Pr^{0.4} \tag{53}$$

Eq. (23) indicates that the fully developed dimensionless radius δ^* of the liquid-solid interface can be related to a single dimensionless parameter ϕ (freezing parameter) for various sets of the Reynolds number and the Prandtl number. The freezing parameter, which depends on the wall temperature and the internal heat generating rate, is defined as $\phi=\theta_w/Q^*=4k(T_f-T_w)/QR^2$. The relationship between $\delta^*$and ϕ is shown in Fig. 2.

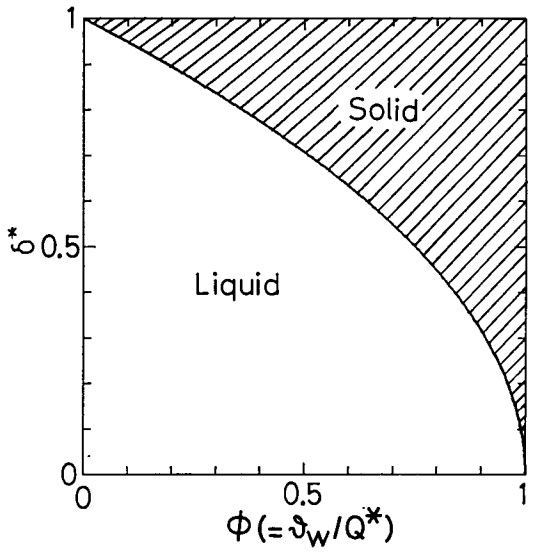

Fig. 2. Effect of freezing parameter on dimensionless solid layer thickness in fully developed region.

It can be seen from the figure that δ^* decreases with increasing ϕ. This means that the lower wall temperature and the lower rate of the internal heat generation form the thicker shell of the solid phase. The flow channel is completely blocked at $\phi=1$. The dependency δ^* on ϕ for the turbulent flow is the same as that for the laminar flow[12].

Fig. 3 shows the fully developed temperature distributions for several values of the Reynolds number. The Prandtl number is taken as 1. In this figure is also

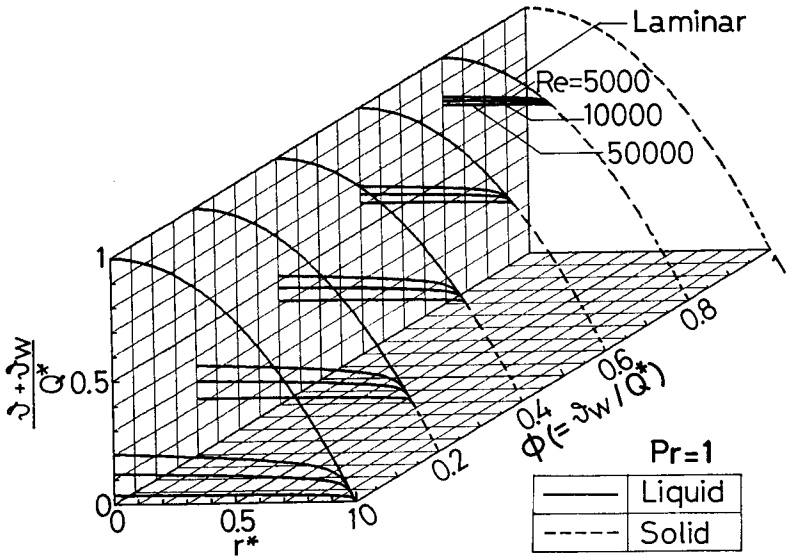

Fig. 3. Effect of Reynolds number on radial dimensionless temparature distribution in fully developed region.

indicated the temperature distribution under the laminar flow condition. The solid and broken lines imply the liquid and solid phases, respectively. The thickness of the solid-phase shell increases with increasing ϕ. In the laminar flow the temperature distribution does not change, and can be described as a parabolic curve in both liquid and solid phases. In the turbulent flow, however, a flat temperature distribution is observed in the liquid phase, and the distribution becomes flatter with an increasing Re since the heat transfer is more enhanced with an increasing Re.

Fig. 4 shows the effect of the Prandtl number on fully developed temperature distributions for $Re=10000$. In the solid phase a parabolic distribution is always observed due to heat conduction. In the liquid phase, however, flat distributions are dominant and the flatness is more accentuated with a higher Pr since the turbulent mixing is more dominant than the heat conduction.

An increase in the Prandtl number yields a decrease in the dimensionless temperature $(\theta+\theta_w)/Q^*$ of the liquid phase for a given value of ϕ. This of course does not indicate an increase in actual heat transfer, but simply that the ratio of actual heat transfer to conductive heat transfer has increased since Q^* varies inversely with changes in the thermal conductivity. The actual heat transfer is decreased due to the lower values of the thermal conductivity resulting from higher Prandtl numbers.

3.2. Thermal entrance region

A dimensionless frozen shell thickness $(1-\delta^*)$ is plotted versus a dimensionless

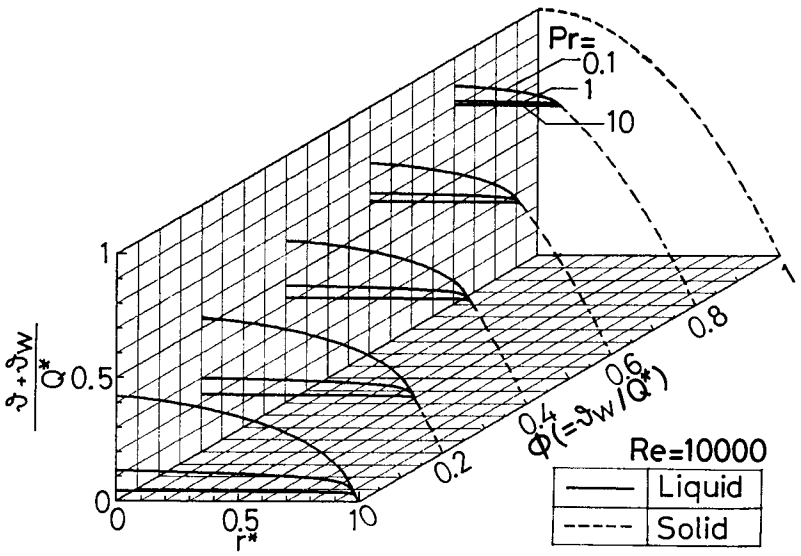

Fig. 4. Effect of Prandtl number on radial dimensionless temperature distribution in fully developed region.

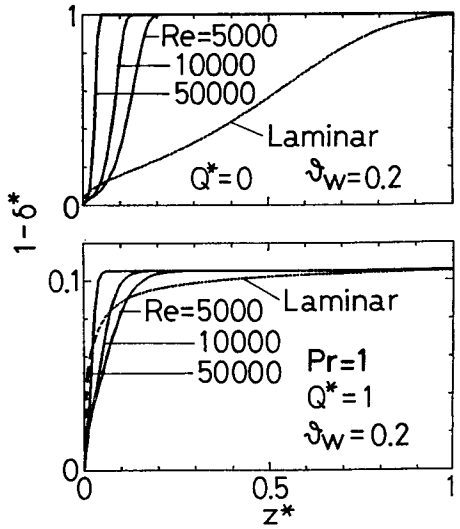

Fig. 5. Effect of Reynolds number on axial distribution of dimensionless solid layer thickness in thermal entrance region.

axial position z^* in Fig. 5 for several turbulent flow cases (having different values of the Reynolds number) as well as for the laminar flow case taken from Ref. 12. The Prandtl number is again chosen as equal to 1. For the heat generating fluid ($Q^*=1$), the thickness of the frozen shell increases with distance down the tube

and then approaches its fully developed value, which depends on the freezing parameter $\phi(=\theta_w/Q^*)$ and is given by Eq. (23). For a given value of z^* an increase in the Reynolds number yields an increase in the frozen shell thickness. This does not indicate an actually rapid growth of the frozen shell since z^* varies inversely with changes in the Reynolds number. For a given tube with a reduced flow area due to freezing, an increase in the Reynolds number enhances the heat transfer, and thus causes the thickness of the frozen shell to be reduced. It is also noted that the turbulent flow frozen shell is thicker than the laminar flow case (with the same z^*). This is because a fully developed condition can be established in a shorter tube for the turbulent flow than for the comparable laminar flow.

In this figure is also indicated the calculated results for a fluid with no heat generation ($Q^*=0$). The growth of the frozen shell is significantly rapid in the non-generating fluid. The shell thickness increases monotonically with an increasing axial length, and the channel is completely blocked at a given position along the tube.

Fig. 6 is a plot of dimensionless solid shell thickness $(1-\delta^*)$ versus z^* for flows of the same Reynolds number ($Re=10000$) but having different values of the Prandtl number. For all cases the thickness of the solid shell again increases with an increasing axial length and then approaches its fully developed value. For a given value of z^*, an increase in the Prandtl number yields an increase in the solid shell thickness.

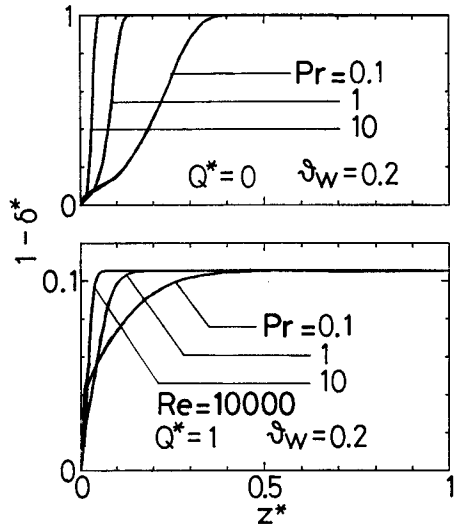

Fig. 6. Effect of Prandtl number on axial distribution of dimensionless solid layer thickness in thermal entrance region.

Fig. 7 shows the axial distributions of the local Nusselt number Nu for several different turbulent flow Reynolds numbers as well as the laminar flow case. The values of Pr and θ_w are taken as 1 and 0.2, respectively. For the heat generating fluid ($Q^*=1$), the turbulent flow Nusselt number first decreases rapidly with an increasing z^*, and then approaches its fully developed value predicted in Eq. (27), which depends on both Re and Pr. Nu becomes higher with a higher Re. All the turbulent flow Nusselt numbers are significantly higher than those for the laminar flow case.

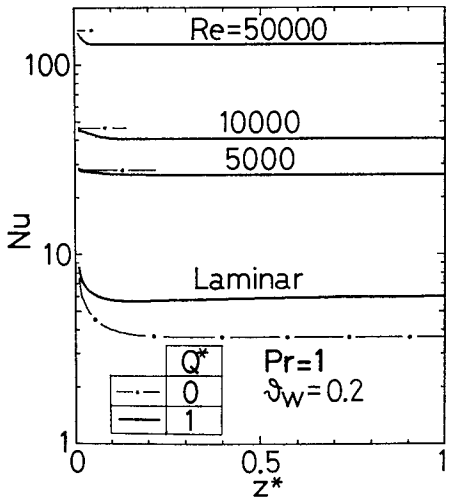

Fig. 7. Effect of Reynolds number on axial distribution of local Nusselt number in thermal entrance region.

For the fluid with no heat generation ($Q^*=0$), the turbulent flow Nusselt numbers are shown only in the short region between the inlet and a given point where the channel is blocked completely.

Fig. 8 shows the effect of the Prandtl number Pr on the axial distributions of the local Nusselt number for fluids with and without heat generation. The values of Re and θ_w are taken as 10000 and 0.2, respectively. Nu increases with a higher Pr since, for high Pr, the turbulent mixing becomes more dominant than the heat conduction.

Fig. 9 shows the radial dimensionless temperature distributions at several positions of the thermal entrance region for the turbulent flow ($Re=10000$) as well as for the laminar flow. Pr and θ_w are taken as 1 and 0.2, respectively. Q^* ranges between 0 and 1. The solid and broken lines represent the liquid and solid temperatures, respectively. In the laminar flow, with an increasing axial length, a flat distribution of liquid temperature is seen to change into a parabolic one observed

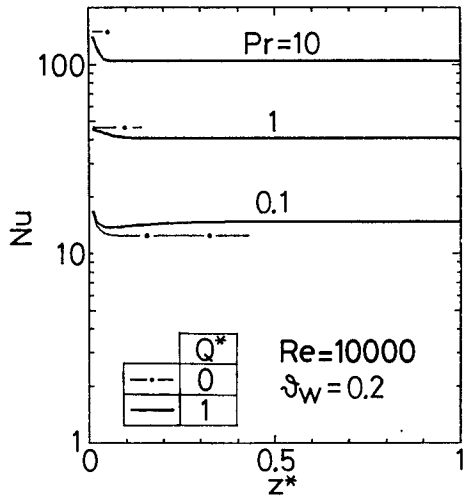

Fig. 8. Effect of Prandtl number on axial distribution of local Nusselt number in thermal entrance region.

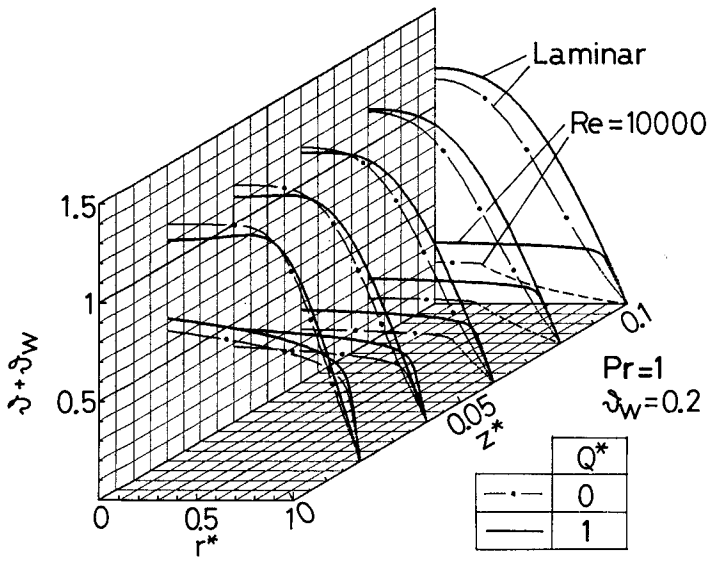

Fig. 9. Effect of Reynolds number on radial dimensionless temperature distribution in thermal entrance region.

in the fully developed region. In the turbulent flow, however, a flat distribution is always observed along the tube because of turbulent mixing.

Fig. 10 shows the radial dimensionless temperature distributions at several positions for flows of the same Reynolds number (Re=10000) but having different values

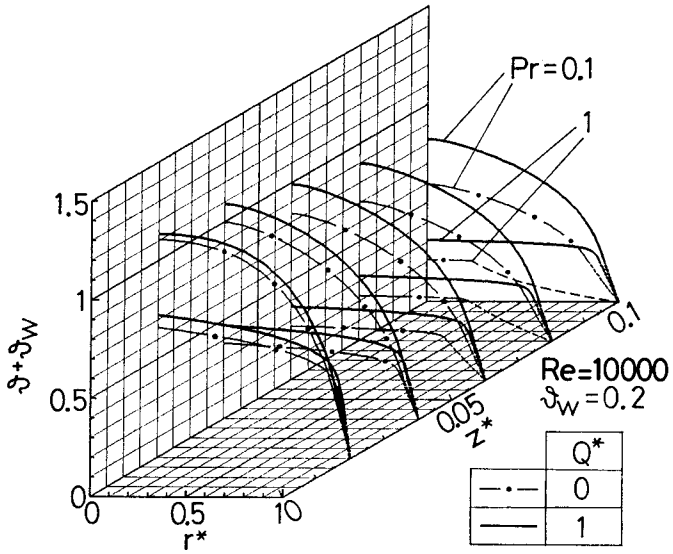

Fig. 10. Effect of Prandtl number on radial dimensionless temperature distribution in thermal entrance region.

of the Prandtl number. For all cases the dimensionless temperature at the tube center decreases with an increasing axial length, and then approaches its fully developed value. An increase in the Prandtl number yields a flatter distribution of the liquid temperature.

Fig. 11 shows the axial distributions of the dimensionless heat transfer rate Q_T*

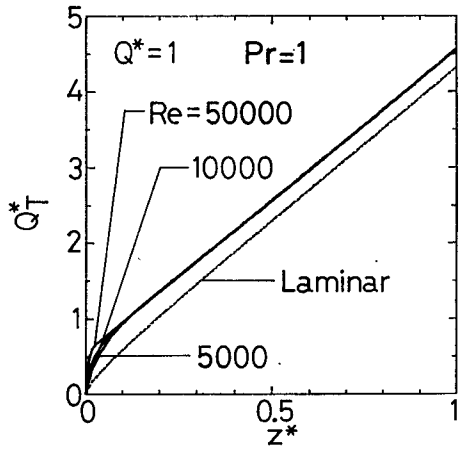

Fig. 11. Effect of Reynolds number on axial distribution of dimensionless heat transfer rate in thermal entrance region.

for several turbulent Reynolds numbers as well as the laminar flow case. Both Q^* and Pr are taken as 1. Q_T^* first increases rapidly and then approaches a straight line, whose gradient is dependent on Q^*. In the turbulent flow, the Q_T^* curves are almost identical over most of the range z^* values considered, the only deviation occurring near the inlet. The values of Q_T^* are independent of θ_w, as defined in Eq. (52). The plots of Q_T^*, therefore, are identical with the non-solidification ones for $\theta_w=0$.

Fig. 12 is a polt of Q_T^* versus z^*, but for the cases involving variations of Pr. It can be seen from the figure that, for a given value of z^*, the turbulent flow dimensionless heat transfer rate Q_T^* is only moderately sensitive to changes in Pr, with in creases in Pr resulting in higher values of Q_T^*.

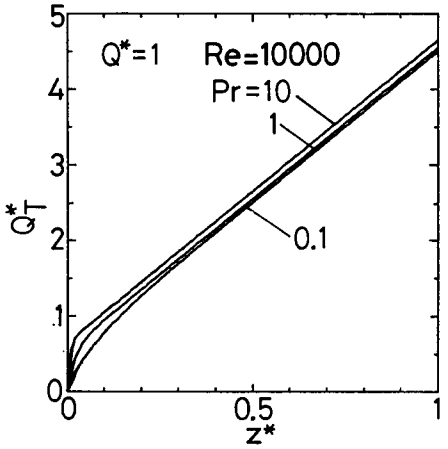

Fig. 12. Effect of Prandtl number on axial distribution of dimensionless heat transfer rate in thermal entrance region.

4. Conclusions

The effect of freezing on the turbulent flow heat transfer characteristics of a liquid with internal heat sources flowing in a cooled circular tube is investigated analytically. Steady-state conditions and a uniform wall temperature, which is lower than the freezing temperature of the liquid, are assumed. The radius of the liquid-solid interface, the local Nusselt number and the heat transfer rate from the wall are determined as a function of position along the tube for various sets of the Reynolds number and the Prandtl number.

(1) The radius of the liquid-solid interface decreases with distance down the tube and approaches its fully developed value predicted easily in Eq. (23), which has only the variable ϕ defined as the relative rate of wall cooling and internal

heating. The fully developed correlation of Eq. (23) for the turbulent flow is the same as that for the laminar flow[12].

(2) The local Nusselt number first decreases rapidly with distance and then approaches its fully developed value, which depends on the Reynolds number and the Prandtl number.

(3) The heat transfer rate from the wall first increases rapidly with distance and then approaches a straight line whose gradient is dependent on the internal heating rate.

Application of the present simple analysis is limited to the case of a thin frozen shell, since the effect of a liquid-solid interface curvature on the structure of turbulent flow is neglected. For a thicker frozen shell case, however, the fluid acceleration due to the change in the flow area may possibly influence the turbulence structure. Hence, further works, both theoretical as well as experimental, are needed. Also, other studies are required for liquid metals with a low Prandtl number.

Appendix. Correlation for turbulent velocity and eddy diffusivity

To obtain the solutions of Eq. (16), it is necessary that the variations of u_0^* and Γ_0 with η^* are specified. A number of attempts have been made to predict the turbulent velocity distribution and the eddy diffusivity of heat. In the present calculation, for simplicity, the eddy diffusivity ε_H of heat is assumed to be equal to the eddy diffusivity ε_M of the momentum, and the following simple equations are used.

$0 \leq y^\dagger \leq 26$ (boundary layer):

$$u_0^\dagger = \frac{1}{0.36}\ln(1+0.36y^\dagger) + 7.2\left[1-\exp\left(-\frac{y^\dagger}{12}\right)-\frac{y^\dagger}{12}\exp(-0.37y^\dagger)\right] \tag{A1}$$

$$\Gamma_0 = 1+0.124^2 u_0^\dagger y^\dagger Pr[1-\exp(-0.124^2 u_0^\dagger y^\dagger)] \tag{A2}$$

$26 \leq y^\dagger$ (center region):

$$u_0^\dagger = \frac{1}{0.36}\ln(y^\dagger/26) + 12.85 \tag{A3}$$

$$\Gamma_0 = 1+Pr[0.36y^\dagger(1-y^\dagger/R^\dagger)-1] \tag{A4}$$

where $y^\dagger$, $R^\dagger$ and u_0 are the dimensionless quantities given by

$$y^\dagger = (R-r)u_\tau/\nu,\quad R^\dagger = Ru_\tau/\nu,\quad u_0^\dagger = u_0/u_\tau,\quad u_\tau = \sqrt{\tau_w/\rho} \tag{A5}$$

The turbulent velocity $u^\dagger_0$ of Eqs. (A1) and (A3) is similar to that given by Deissler[14] but having a modified form. The total thermal diffusivity Γ_0 of Eqs. (A2) and (A4) is taken from Sparrow et al[15].

Acknowledgements

The authors are grateful to Prof. I. Michiyoshi, Kyoto University, for his valuable suggestions throughout the study. This work was partly supported by the

Ministry of Education, Science and Culture through the Scientific Research Grant.

Nomenclature

a thermal diffusivity
c specific heat
c_n coefficient defined by Eq. (44)
k thermal conductivity
Nu local Nusselt number $(=2\alpha\delta/k)$
Pr Prandtl number $(\nu=/a)$
Q internal heat generating rate per unit volume
Q^* dimensionless internal heat generating rate $(=QR^2/4k(T_0-T_f))$
q heat flux
q^* dimensionless heat flux $(=qR/k(T_0-T_f))$
Q_T heat transfer rate
Q_T^* dimensionless heat transfer rate $(=Q_T/\pi R^2 c\rho u_{m0}(T_0-T_f))$
R radius of tube
r radial coordinate
r^* dimensionless radial coordinate $(=r/R)$
Re Reynolds number $(2u_{m0}R/\nu)$
T temperature
T_f freezing temperature of liquid
u velocity
u^* dimensionless velocity $(=u/u_{m0})$
$u^\dagger$ dimensionless velocity $(=u/u_\tau)$
u_τ friction velocity $(=\sqrt{\tau_w/\rho})$
y distance from wall $(=R-r)$
$y^\dagger$ dimensionless distance $(=yu_\tau/\nu)$
z axial coordinate
z^* dimensionless axial coordinate $(=2z/RePrR)$

Greek letters

α heat transfer coefficient $(=q/(T_m-T_f))$
Γ dimensionless total thermal diffusivity defined in Eq. (9)
δ radius of liquid-solid interface
δ^* dimensionless radius of liquid-solid interface $(=\delta/R)$
ε_H eddy diffusivity of heat
ε_M eddy diffusivity of momentum
η dimensionless radial coordinate $(=r/\delta)$
θ dimensionless temperature $(=(T-T_f)/(T_0-T_f))$

θ_w dimensionless wall temperature $(=(T_f-T_w)/(T_0-T_f))$

λ_n eigen-value

ν kinematic viscosity

ρ density

ϕ dimensionless freezing parameter $(=4k(T_f-T_w)/QR^2)$

ψ_n eigen-function

Subscripts

l liquid

m mean condition

s solid

w inside surface of tube wall

0 inlet condition

Superscripts

e thermal entrance region

fd fully developed region

$*$ dimensionless quantity

References

1) L. E. McNeese; ORNL-TM-3141 (1971).
2) M. J. Monsler et al.; Nucl. Technol./Fusion; **1**, 302 (1981).
3) R. D. Zerkle and J. E. Sunderland; J. Heat Transfer; **90**, 183 (1968).
4) M. N. Özisik and J. C. Mulligan; J. Heat Transfer; **91**, 385 (1969).
5) J. C. Mulligan and D. D. Jones; Internat. J. Heat Mass Transfer; **19**, 213 (1976).
6) S. B. Thomason et al.; J. Heat Transfer; **100**, 387 (1978).
7) C. Cho and M. N. Özisik; J. Heat Transfer; **101**, 465 (1979).
8) R. R. Gilpin; J. Heat Transfer; **103**, 363 (1981).
9) M. S. Sadeghipour et al.; Nucl. Sci. Eng.; **79**, 9 (1981).
10) P. Sampson and R. D. Gibson; Internat. J. Heat Mass Transfer; **24**, 231 (1981).
11) N. Seki et al.; J. Heat Transfer; **106**, 498 (1984).
12) Y. Kikuchi and Y. Shigemasa; Nucl. Eng. Design; **75**, 73 (1982).
13) F. W. Dittus and L. M. K. Boelter; Univ. Calif., Pubs. Eng.; **2**, 443 (1930).
14) R. G. Deissler; NACA Rep. 1210 (1955).
15) E. M. Sparrow et al.; App. Sci. Res., Sec. A; **7**, 37 (1957).